Temperature-Dependent Structure of α-CD/PEO-Based Polyrotaxanes in Concentrated Solution in DMSO: Kinetics and Multiblock Copolymer Behavior

Christophe Travelet,[†,||] **Pascal Hébraud,**[‡] **Christophe Perry,**[†] **Cyril Brochon,**[†,⊥] **Georges Hadziioannou,**[†,⊥] **Alain Lapp,**[§] **and Guy Schlatter*,**[†]

[†]*Laboratoire d'Ingénierie des Polymères pour les Hautes Technologies, EAC 4379, CNRS, Université de Strasbourg, ECPM, 25 rue Becquerel, 67087 Strasbourg cedex 2, France,* [‡]*Institut de Physique et Chimie des Matériaux de Strasbourg, CNRS UMR 7504, Université de Strasbourg, 23 rue du Loess, BP 43, 67034 Strasbourg cedex 2, France, and* [§]*Laboratoire Léon Brillouin, CEA Saclay, 91191 Gif-sur-Yvette cedex, France.* [||]*Current address: Centre de Recherches sur les Macromolécules Végétales, CNRS UPR 5301, Université Joseph Fourier de Grenoble, BP 53, 38041 Grenoble cedex 9, France.* [⊥]*Present address: Laboratoire de Chimie des Polymères Organiques, CNRS UMR 5629, Université de Bordeaux, 16 avenue Pey Berland, 33607 Pessac cedex, France.*

ABSTRACT: The structure of polyrotaxanes (PRs) based on α-cyclodextrins (α-CDs) threaded onto 22 kg mol^{-1} poly(ethylene oxide) (PEO) chains in concentrated solution ($\approx$20% w/w) in dimethyl sulfoxide (DMSO) was studied by small-angle neutron scattering (SANS) measurements as a function of the temperature and the complexation degree N (i.e., the number of threaded α-CDs per PR which ranged from 7 up to 157). A multiblock copolymers behavior was revealed for PRs in DMSO. This multiblock behavior of PRs at 43 °C is due to the presence of two kinds of blocks which alternate along the PR. One block type is rigid and corresponds to α-CD rodlike tubes with a length $L_{rod} \approx 7$ nm. The other block type corresponds to flexible naked PEO segments. When the PR mixtures are cooled down to 21 °C, they gelify slowly with time and form transparent physical gels. The gel structure is due to the multiblock copolymer behavior of PRs leading to the formation of regular bundles for which the characteristic sizes ($L = 14$ nm and $R = 5.7$ nm) are constant during the gelation process and are independent with N. These regular bundles contain naked PEO segment crystallites surrounded by α-CD rodlike tube aggregates at their extremities. Indeed, α-CD rodlike tubes, which are present in the initial state at 43 °C, act like a compatibilizer and thus lead to the nanoscale bundle sizes and thus to the transparency of the physical PR-based gels. Furthermore, we showed that the kinetics of the bundle formation is N-dependent. Indeed, at constant PR weight fraction in DMSO, the N value is a crucial parameter controlling the intrinsic flexibility of PRs (flexibility favored at low N values) and their prealignment (prealignment favored at high N values) and thus controlling the self-organization.

1. Introduction

Polyrotaxane (PR) is a pearl necklace shape supramolecule in which many macrocycles (the pearls) are threaded onto a single template polymer chain (the necklace). The ends of the template chain are capped with steric functional groups to prevent dethreading of the macrocycles.[1,2] The translational and rotational mobility of the macrocycles along the template chains confer new dynamical, physicochemical, and mechanical properties on the PRs. These macromolecules open the door to the realization of new functional materials. Among them, high swelling gels exploit the mobility of the macrocycles along the template chains. The macrocycles are covalently cross-linked in an intermolecular way and form a chemical gel whose cross-link points may freely slide along the template chains. This supplementary degree of freedom leads to high swelling ratios and to original viscoelastic properties of the gels.[3−9] Nanowires, as for them, utilize the topological separation induced by the macrocycles between their interior and exterior. Indeed, their aligning along template polymer chains creates transient tubes. PRs with semiconducting polymers as template chains have thus been synthesized and used as single-molecule nanowires.[10,11] Finally, drug delivery systems based on PRs have been synthesized. A high number of proteins, covalently linked onto

the macrocycles, are conveyed to the appropriate biological receptors and then released after hydrolysis of the template chains.[12]

Many types of macrocycles and template chains can be used, leading to a huge number of different PRs. Among them, PRs formed with α-cyclodextrins (α-CDs) as macrocycles and poly(ethylene oxide) (PEO) as template chains have been widely studied.[13] α-CDs consist in the repetition of six glucose units organized in a truncated conic way. The threading between α-CDs and PEO is possible due to a negative Gibbs free energy change during the threading process. The difference of Gibbs free energy, determined both theoretically and experimentally, is equal to -50 kJ mol^{-1}.[14,15]

Nevertheless, the representation of PRs as molecular pearl necklaces in which the macrocycles freely slide along the template chains is much too simplistic. It ignores the numerous interactions that develop between each component of PRs when put into solution. The complexity introduced by the interplay of the interactions between the components manifests itself by the difficulty to solubilize PRs. Thus, PRs based on α-CDs and PEO are insoluble in neutral water or *N,N*-dimethylformamide, even though both are good solvents of the macrocycles and the template chains. Limited solubility has been empirically observed in few solvents, such as dimethyl sulfoxide (DMSO),[16,17] aqueous NaOH solution (thanks to the ionization of α-CD hydroxyl groups

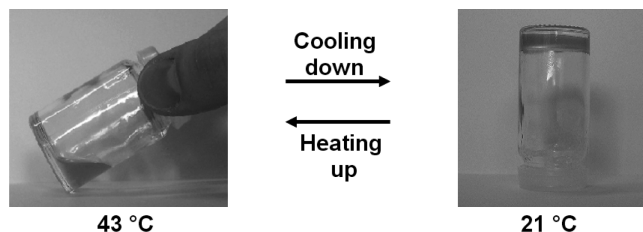---

*Corresponding author. E-mail: Guy.Schlatter@unistra.fr.

Figure 1. Thermoreversible gelation of PR$_{85}$ at 19.6% w/w in DMSO: liquid state at 43 °C and gel state after 24 h at 21 °C.

whose p$K_a \approx 12$),[16,17] halogen-containing ionic liquids,[18] concentrated aqueous solutions of calcium thiocyanate,[19] and *N,N*-dimethylacetamide/lithium halogenide mixtures.[20] Among them, DMSO has been the most used.

Nevertheless, although a concentrated mixture of PR in DMSO is fluid at high temperature, when it is cooled down to room temperature, it becomes a physical gel (Figure 1).[21] Moreover, at room temperature, mixtures of PR in DMSO exhibit a thixotropic rheological behavior.[22,23] These observations indicate that microscopic physical aggregates are formed and may be broken by heating or by the application of a shear.

We have already studied the self-organization of PRs in DMSO at room temperature in the steady state and shown that association between α-CDs as well as between naked PEO segments (i.e., the ethylene oxide units of the PEO chains which are not covered by α-CDs) is present.[21] However, in this paper we adjusted the model and studied the gelation kinetics of mixtures of PR in DMSO and more particularly the formation of α-CD aggregates and naked PEO segment crystallites by means of neutron scattering experiments.

2. Experimental Section

2.1. Material Preparation and Polyrotaxane Synthesis. Material preparation and α-CD/PEO-based PR synthesis were carried out according to an already published procedure.[24] In particular, α,ω-bis-amine-terminated PEO was synthesized from commercial dihydroxy-terminated PEO according to an adaptation of the procedure of Mutter.[25] Dihydroxy-terminated PEO with an average number molecular weight of 22 kg mol^{-1} and a polydispersity index of 1.03 (as measured in DMSO at 70 °C by gel permeation chromatography with PEO standard calibration) was used as template chain and 2,4-dinitro-1-fluorobenzene as steric functional group. The values of the PR complexation degree were estimated using ^{1}H nuclear magnetic resonance in deuterated dimethyl sulfoxide with a 99.9% enrichment (DMSO-d_6)[24] and the efficiency of the capping step using gel permeation chromatography in HPLC grade DMSO at 70 °C.[24]

2.2. Small-Angle Neutron Scattering (SANS). SANS measurements were performed on the PAXY spectrometer at the Laboratoire Léon Brillouin (LLB, CEA, Saclay, France). The modulus of the scattering vector is denoted q and is equal to $(4\pi/\lambda)$ sin$(\theta/2)$, where θ designates the observation angle and λ represents the wavelength of the radiation used. The first spectrometer configuration (second spectrometer configuration) consisted of a sample-to-detector distance of 3 m (1 m) and a wavelength of 1.0 nm (0.6 nm). The global probed q range corresponding to these configurations was 8.0×10^{-2} nm$^{-1} \leq q \leq 3.5$ nm^{-1}. The signal was corrected by taking into account the contributions of the measurement cell, the solvent, and the incoherent background.[26] The incoherent scattering of poly-(methyl methacrylate) was used to correct the detector efficiency. Thus, the data were brought to absolute scale. The measurement cells were made of 1 mm thick quartz windows separated by a 2 mm O-ring and equipped with a cadmium/boron carbide diaphragm whose hole diameter is 10 mm. DMSO-d_6 was used as the solvent during all of the experiments. The temperature-regulated rack carrying the measurement cells filled in with the

PR solutions was heated up at 43 ± 1 °C, and one 30 min scan was measured at that temperature. Then, the solutions were cooled down at 21 ± 1 °C, and 30 min scans were continuously recorded during few hours at this temperature.

3. Results and Discussion

PRs with well-defined complexation degrees (N) (i.e., the number of threaded α-CDs per PEO chain) ranging from 7 to 157 (Table 1) were obtained thanks to the methodology previously reported.[24] In this paper, the PRs will be denoted PR$_N$, where N is the complexation degree. PEO with a molecular weight of 22 kg mol^{-1} was used. Thus, the α-CD overlap ratio (i.e., the percentage of ethylene oxide units of the PEO chains which are covered by α-CDs) ranges from 3% to 63% (Table 1). A concentrated PR mixture in DMSO heated up at 43 °C is fluid. When cooled down to 21 °C, it gelifies slowly with time (Figure 1). This process seems to be fully thermoreversible as the formed gel returns to its original fluid state and remains fluid when heated up at 43 °C. Before considering the gelation of the PR solutions at 21 °C, we determined first the initial structure of the systems out of the gel state, i.e., at 43 °C.

3.1. Structure of Polyrotaxanes in Concentrated Solution at 43 °C. Before studying PRs themselves at 43 °C, we first focus on pure PEO (i.e., PR$_0$) in solution in DMSO-d_6. A 5.9% w/w PEO solution was chosen so as to have the same mole number of naked ethylene oxide units as in a PR$_{37}$ solution at 19.6% w/w (Table 1). Small-angle neutron scattering (SANS) measurements do not show any structural evolution of the PEO solution with time at 43 °C. A perfect Gaussian behavior is observed (Figure 2), and the corresponding gyration radius is $R_g = 2.6$ nm. SANS measurements do not show any structural evolution of all PR solutions with time at 43 °C. The scattering profiles of the PR solutions, except PR$_{157}$, exhibit several features (Figure 2):

• For the highest q values (up to 3.5 nm^{-1}), a q^{-1}-like behavior of the scattering intensity without oscillation is obtained. This suggests the presence of thin α-CD rodlike tubes.

• For the lowest q values (down to 8.0×10^{-2} nm^{-1}), an excess of scattering intensity is observed. This behavior is due to the presence, at the molecular level, of regions more or less concentrated in naked PEO segments (i.e., the ethylene oxide units of the PEO chains which are not covered by α-CDs) and/or in α-CD rodlike tubes depending on the N value. Furthermore, these regions exhibit a fractal characteristic dimension close to 2 (i.e., close to a Gaussian arrangement).

To confirm this interpretation, the experimental curves have been fitted with the following model which is a linear combination of a cylinder form factor P_{cyl}[30,31] and a Gaussian form factor P_{Gauss}:[31,32]

$$I(q) = A_{rod} \exp\left[-\left(\frac{q}{q_0}\right)^{5.33}\right] P_{Gauss}(q, R_{ghost})$$

$$+ B_{rod}\left\{1 - \exp\left[-\left(\frac{q}{q_0}\right)^{5.33}\right]\right\} P_{cyl}(q, L_{rod}, R_{rod}) + I_{inc} \quad (1)$$

where $I(q)$ is the scattering intensity at the modulus of the scattering vector q and I_{inc} is the constant intensity of a reminiscent incoherent signal. L_{rod} and R_{rod} respectively designate the cylinder length and radius, and R_{ghost} designates the gyration radius of the Gaussian distribution of α-CD rodlike tubes (the cylinders) and/or naked PEO segments. The weighting of each form factor is a cutoff function so that P_{cyl} dominates at $q > q_0$ and P_{Gauss} dominates at $q < q_0$.

Table 1. Chemical Characteristics of the PEO Solution at 5.9% w/w and of PR Solutions at 19.6% w/w in DMSO[a]

PR_N	α-CD overlap ratio [%][b]	$n(PR_N)$ [mmol]	$n(PR_N)/$ $n(PR_{157})$	$n(\alpha\text{-CD})$ [mmol]	$n(\alpha\text{-CD})/$ $n(\alpha\text{-CD})PR_7$	n(naked PEO units) [mmol][b]	n(naked PEO units)/ n(naked PEO units)$_{PR157}$[b]
PEO = PR$_0$	0	0.28	2.54			142	6.82
PR$_7$	2.80	0.68	6.06	4.76	1	330	15.9
PR$_{37}$	14.8	0.34	3.01	12.5	2.63	144	6.91
PR$_{85}$	34.0	0.19	1.67	15.9	3.34	61.7	2.97
PR$_{157}$	62.9	0.11	1	17.6	3.70	20.8	1

[a] The given mole numbers refer to 100 g of solution. [b] Calculated taking into account that one α-CD covers exactly two ethylene oxide units of PEO,[27,28] although a higher α-CD coverage was recently reported.[29]

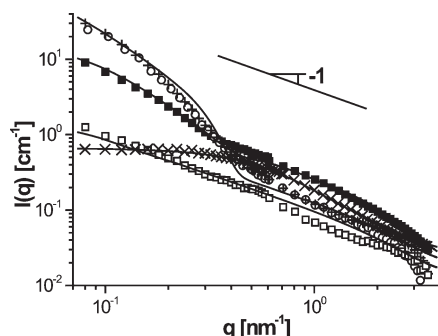

Figure 2. SANS: absolute scattering intensity $I(q)$ versus modulus of the scattering vector q for (×) pure PEO (i.e., PR$_0$) at 5.9% w/w in DMSO-d_6 at 43 °C and PR solutions at 19.6% w/w in DMSO-d_6 at 43 °C: (■) PR$_7$, (○) PR$_{37}$, (+) PR$_{85}$, and (□) PR$_{157}$. The solid line corresponding to PEO is the fitting curve obtained with a Gaussian form factor. The solid lines corresponding to PRs are the fitting curves obtained with eq 1.

Table 2. Fitting Parameters Obtained for PR$_N$ Solutions at 43 °C

PR_N	q_0 [nm^{-1}]	R_{ghot} [nm]	L_{rod} [nm]	R_{rod} [nm]
PR$_7$	0.45	18	7	0.73
PR$_{37}$	0.35	30	10	0.73
PR$_{85}$	0.35	30	10	0.73
PR$_{157}$			50	0.73

Figure 2 shows a good accuracy between the experimental and the calculated profiles with $L_{rod} \geq 7$ nm and $R_{rod} = 0.73 \pm 0.1$ nm (Table 2) which corresponds to the radius of one α-CD.[33] Only a minimum value of L_{rod} can be estimated due to the predominance of the Gaussian part of the intensity at the lowest measured q values. The obtained parameters L_{rod} and R_{rod} confirm that PRs in concentrated solution at 43 °C contain rodlike tubes consisting of weakly stacked α-CDs along the PEO chains (Figure 3). This is in agreement with a study carried out on chemically linked α-CD tubes[34] where it is found both theoretically and experimentally that α-CD tubes are constituted by 2−7 α-CDs. This is also consistent with a SANS observation of uncapped PRs in the solid state.[35] This is likewise in agreement with a recent theoretical study[36] in which it is shown using Monte Carlo simulations that α-CDs are stacked by groups of 3−4 α-CDs. Thus, knowing that the length of an α-CD is 0.79 nm,[33] the value of L_{rod} is relatively high compared to the above given data taken from the literature. Nevertheless, this is explained by the presence of ethylene oxide units between α-CD rodlike tubes, both being observed by SANS (see Supporting Information). Furthermore, the dynamic character of the α-CD rodlike tubes at high temperature (43 °C) can explain the high value of L_{rod}. Indeed, the dynamic character is due to the mobility of the α-CDs along the PEO chains in DMSO[7,37] and to continuously forming and breaking weak connections between two neighboring α-CDs belonging to the same PR or not (Figure 3). Such dynamics was not observed for similar systems in the semidilute regime.[38] However, PRs
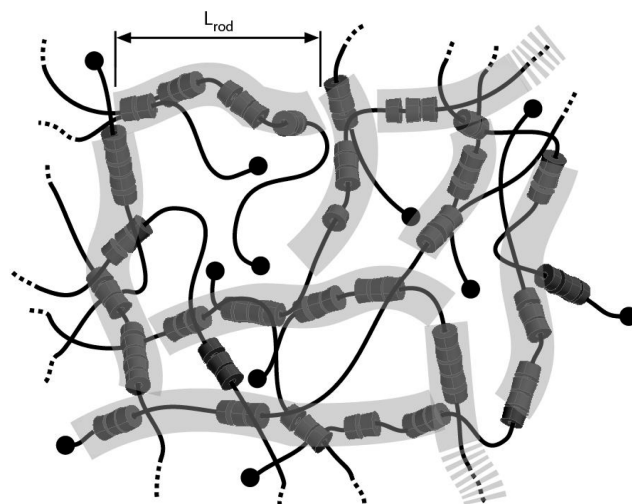

Figure 3. Schematic representation of the liquid state at 43 °C of a concentrated PR$_N$ solution in DMSO for intermediate N values. The transparent thick lines represent the α-CD rodlike tubes of length L_{rod} as shown by SANS. The figure shows isolated α-CD rodlike tubes and also regions more dense in α-CD rodlike tubes.

were studied at room temperature and modified with hydroxypropyl groups weakening hydrogen bonds between α-CDs. Moreover, a solvation effect due the fact that α-CD hydroxyl groups are not naked but surrounded by bounded DMSO molecules increases the L_{rod} value. Finally, the α-CD dynamics of our PR systems leads to quite a high L_{rod} value.

For the less threaded PR (PR$_7$), the fitting shows a very good accuracy with the experimental curve. This confirms the cohabitation of isolated α-CD rodlike tubes surrounded by DMSO (intensity contribution for $q > q_0$) and long naked PEO segments organized in a Gaussian way (intensity contribution for $q < q_0$). Indeed, PR$_7$ has an α-CD overlap ratio of 3%, and its solution contains 16 times more naked PEO units compared to PR$_{157}$ (Table 1). The obtained results show that regions, with a characteristic radius of $R_{ghot} = 18$ nm, contain few long naked PEO segments belonging to different PR$_7$ molecules. However, such regions contain a high amount of solvent and cannot be seen as compact aggregates.

The scattering profile of the PR$_{157}$ solution is different from the scattering profiles of the three other solutions discussed above. Indeed, the expected excess of scattering intensity does not appear in Figure 2 but should be observed at smaller q values than the probed ones. Furthermore, it exhibits a q^{-1}-like behavior in the whole probed q range (Figure 2). Fitting with eq 1 confirms these observations and leads to $L_{rod} > 45$ nm, $R_{rod} = 0.73$ nm, and a very low cutoff value $q_0 < 0.08$ nm^{-1}. As for the other studied PRs, PR$_{157}$ contains rodlike tubes consisting of weakly stacked α-CDs along its PEO chain. Nevertheless, the structures formed by the α-CDs are much more rigid than those formed in the PR$_7$, PR$_{37}$, and PR$_{85}$ solutions due to the presence of smaller naked PEO segments between the rodlike tubes.
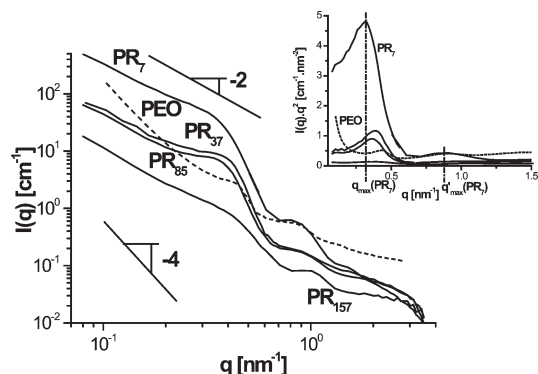
Figure 4. SANS: absolute scattering intensity $I(q)$ versus modulus of the scattering vector q for pure PEO (i.e., PR_0) at 5.9% w/w in DMSO-d_6 after 24 h at 21 °C and PRs at 19.6% w/w in DMSO-d_6 after 8 h at 21 °C: PR_7, PR_{37}, PR_{85}, and PR_{157}. Inset: corresponding Kratky plots. The dotted lines show the q_{max} and q'_{max} positions of the PR_7 peaks.

Consequently, all these SANS observations of PRs in solution in DMSO at 43 °C confirm that PRs can be considered as multiblock copolymers where one block type is made of an α-CD rodlike tube and the other one of a naked PEO segment. The state at 43 °C corresponds to the initial state of the physical gelation observed with time at room temperature. Now, starting from a liquid PR/DMSO mixture at 43 °C, we are going to discuss the PR structure evolution with time at 21 °C, i.e., during the physical gelation.

3.2. Structure Formation with Time of Polyrotaxanes in Concentrated Solution at Room Temperature. SANS measurements were used to resolve the structure of the system as a function of time. It should be remembered at that point that SANS measurements in DMSO-d_6 probe α-CD and PEO in an equivalent way (see Supporting Information).

Before studying PRs themselves, we first focus on pure PEO (i.e., PR_0) in solution in DMSO-d_6. The initial transparent PEO/DMSO solution observed at 43 °C in the previous section is not liquid anymore and appears opaque and heterogeneous to the eyes (with aggregate characteristic size less than 1 mm) after a long time (typically 24 h) at 21 °C. After gelation, the SANS profile of the PEO/DMSO mixture shows three ripples (Figure 4). In the corresponding Kratky plot, shoulders appear like peaks indicating the presence of PEO-based structures interacting between themselves. The q positions of the low q and high q peaks, respectively q_{max} and q'_{max}, are $q_{max} = 4.31 \times 10^{-1}$ nm^{-1} and $q'_{max} = 8.89 \times 10^{-1}$ nm^{-1} (inset, Figure 4). Moreover, the scattering intensity exhibits a q^{-4}-like behavior for the lowest q values (Figure 4). Such a Porod behavior[39−42] shows that the sample is highly heterogeneous and contains large PEO-based aggregates having sharp boundaries, i.e., small interphases between the aggregates, on the one hand, and the solvent and few nonaggregated PEO molecules, on the other hand. This result confirms calorimetric and X-ray scattering measurements showing the presence of PEO crystallites.[21] Furthermore, the large aggregates are constituted by the gathering of smaller entities characterized by the structural peaks observed at q_{max} and q'_{max} (i.e., corresponding to a typical characteristic size of $2\pi/q_{max} \approx 14.6$ nm as far as concerns q_{max}).

The SANS signature of pure PEO at 21 °C being now well established, we focus on PRs. It should be mentioned that, contrary to pure PEO, the physical gels based on PRs are homogeneous to the eyes. SANS experiments were performed on PR_7, PR_{37}, PR_{85}, and PR_{157} solutions at 19.6% w/w in DMSO-d_6, and the resulting gelations were
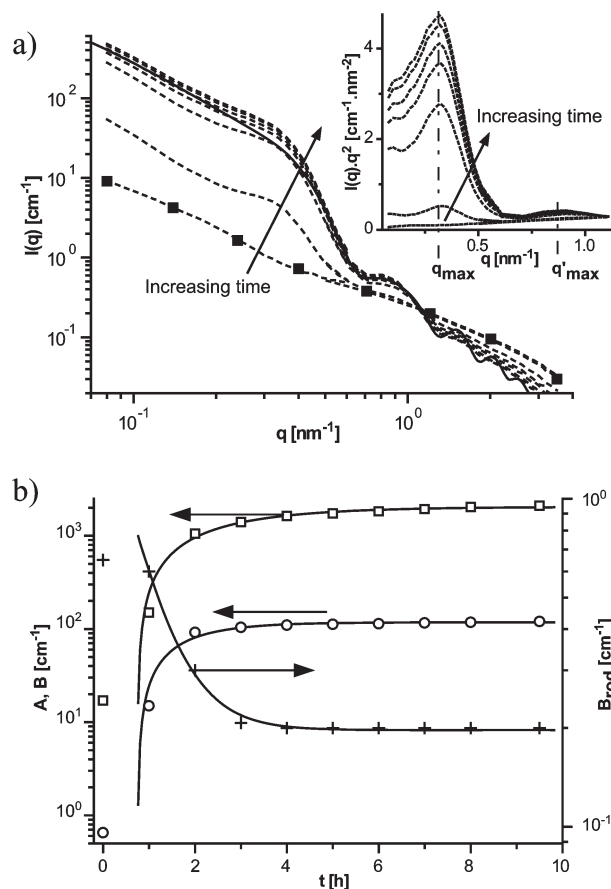

Figure 5. SANS: (a) Absolute scattering intensity $I(q)$ versus modulus of the scattering vector q for PR_7 at 19.6% w/w in DMSO-d_6: (■) at 43 °C (dashed lines) after 0, 1, 2, 3, 4, 6, and 8 h at 21 °C and (solid line) fitting curve with eq 2 of the experimental profile obtained after 4 h at 21 °C. For clarity reasons, only 4 points per decade are shown in the curve at 43 °C. Inset: corresponding Kratky plot. (b) (□) Parameter A which reflects the weight of the Gaussian form factor; (○) parameter B which reflects the weight of the cylinder form factor and (+) parameter B_{rod} which reflects the weight of the rodlike tube form factor as indicating in eq 2 versus time t at 21 °C for PR_7 at 19.6% w/w in DMSO-d_6. The solid lines are the fitting curves obtained with eq 4.

observed with time at 21 °C, the origin of the times being chosen at the moment when the temperature 21 °C is reached.

At Lower Complexation Degree N. As far as concerns the PR_7 solution, from a qualitative point of view, the SANS profiles exhibit the development with time of three ripples during gelation (Figure 5a). In the corresponding Kratky plot, the two main shoulders appear like two peaks. The q positions of the low q and high q peaks, respectively q_{max} and q'_{max}, are $q_{max} = 3.20 \times 10^{-1}$ nm^{-1} and $q'_{max} = 8.75 \times 10^{-1}$ nm^{-1} and do not evolve with time as soon as the gelation starts (inset, Figure 5a). It suggests that association takes place in the form of interactive structures having the same characteristic sizes at any time. However, the q_{max} value obtained with PR_7 is different from the one obtained with pure PEO, suggesting that the presence of few threaded α-CDs (overlap ratio of $PR_7 \approx 3\%$, Table 1) considerably influences the structure size and thus the self-organization behavior itself. Moreover, it should be noticed that the solubilization of PR_7 at room temperature is very easy to carry out although a PEO/DMSO mixture at equivalent concentration cannot be solubilized at room temperature. Thus, the threaded α-CDs play an important role on the formed structure and the macroscopic behavior. For the

lowest q values, an increase of the scattering intensity with time and a q^{-2}-like Gaussian behavior are observed. Furthermore, the intensity of the peaks at q_{max} and q'_{max} increases with time. This indicates that the number of structures increases with time. However, a decrease of the scattering intensity with time is observed at the highest q values, i.e., in the region where a q^{-1}-like behavior of the scattering intensity appears. This latter result tends to show that the proportion of isolated α-CD rodlike tubes decreases with time. All these observations suggest that regular structures containing naked PEO segment crystallites surrounded by α-CD aggregates are formed during gelation and organized in a Gaussian way.

To have more insight into formed structures during time, we propose to model the scattering intensity curves. We showed that during gelation the system can be viewed as a blend of regular structures (called in the following bundles) containing naked PEO segment crystallites surrounded by α-CD aggregates and both isolated naked PEO segments and α-CD rodlike tubes. Thus, the scattering intensity is the sum of the intensity scattered by the isolated entities (naked PEO segments and α-CD rodlike tubes) and the one scattered by the bundles organized in a Gaussian way:

$$I(q) = I_{bundle}(q)$$

$$+ B_{rod}\left\{1 - \exp\left[-\left(\frac{q}{q_0}\right)^{5.33}\right]\right\} P_{cyl}(q, L_{rod}, R_{rod}) + I_{inc} \quad (2)$$

where I_{bundle} is defined as follows:

$$I_{bundle}(q) = A\exp\left[-\left(\frac{q}{q_0}\right)^{5.33}\right] P_{Gauss}(q, R_g)$$

$$+ B\exp\left\{1 - \exp\left[-\left(\frac{q}{q_0}\right)^{5.33}\right]\right\} P_{cyl}(q, L, R) \quad (3)$$

It should be noticed that experimental curves cannot be fitted by any model of spherical symmetry (either a homogeneous sphere model, a spherical core–shell particle model, or a spherical shell particle model). The parameters L_{rod}, R_{rod}, and q_0 are kept equal to the values given by the fitting with eq 1 of the experiments carried out at 43 °C, corresponding to $t = 0$ at 21 °C. Regarding I_{bundle}, the parameters L, R, and R_g are kept equal to the values given by the fitting with eq 3 of the steady state SANS profiles: the bundle length is $L = 14$ nm, the bundle radius is $R = 5.7$ nm, and the gyration radius R_g is estimated to be higher than 33 nm. The weighting of each form factor is a cutoff function so that P_{cyl} dominates at $q > q_0$ and P_{Gauss} dominates at $q < q_0$. It should be noticed that this cutoff function is empiric and allows to model the q domain for which bundles interact between themselves. In fact, the intensity should take into account a structure factor ($I(q) = AS(q)P(q)$). However, an analytical expression of $S(q)$ cannot be obtained for our systems. Thus, the empiric cutoff function has been considered to model the intermediate domain. All following fits consist in determining the weighting of each form factor A, B, and B_{rod} at any given time, all other parameters being kept constant.

Figure 5a shows a good agreement between the fitting curves obtained with the help of eqs 2 and 3 and the experimental data. This confirms that the structural parameters do not evolve with time. Consequently, the characteristic
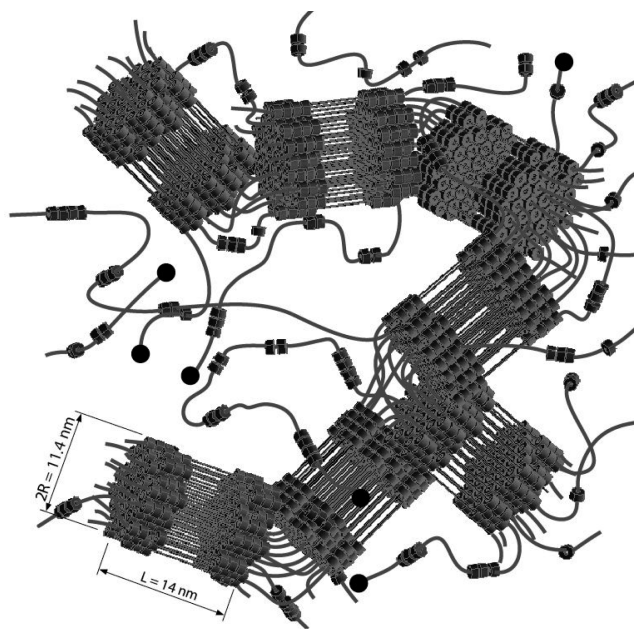

Figure 6. Schematic representation of the gel state after a long aging time (typically 24 h) at 21 °C of a concentrated PR solution in DMSO. Bundles result from naked PEO segment crystallites bounded to their extremities with aggregated α-CD rodlike tubes (these tubes consist of weakly stacked α-CDs along a PEO chain). A certain number of single (not self-assembled) α-CD rodlike tubes are still present. Only few PEO chains are represented for clarity reasons.

bundle length L and radius R are constant at any time. In other words, SANS measurements do not allow to observe the growing of the aggregating bundles with time. On the contrary, the absolute value of the scattering intensity, as the weighting parameters A and B, increase with time (Figure 5b), reflecting the increasing number of aggregated bundles. We conclude the time necessary to form one bundle is much lower than the scan duration of SANS measurements, i.e., 30 min. Furthermore, Figure 5b shows a decrease of B_{rod} with time pointing out the decreasing number of α-CD rodlike tubes with a kinetics having the same characteristic time as for parameters A and B. It should be noticed that introducing the form factor of isolated α-CD rodlike tubes in eq 2 improves significantly the fitting of the experimental data, especially for $q > 1$ nm^{-1}. At long aging time, i.e., once the steady state is reached, $B_{rod} > 0$, suggesting that a fraction of α-CD rodlike tubes is not aggregated and is still present in the system.

The fitting procedure led to estimate the bundle sizes ($L = 14$ nm and $R = 5.7$ nm). From the literature, an α-CD rodlike tube consists of 2−7 α-CDs,[7,34−36] and its length goes from 1.6 to 5.5 nm, which is much less than the bundle length L. Thus, a possible structure of the bundles is a naked PEO segment crystallite bounded to its extremities with aggregated α-CD rodlike tubes (Figure 6). The α-CD rodlike tubes are oriented toward DMSO and play the role of a compatibilizer inducing the nanoscale bundle size and in that way the transparency to the eyes of the physical PR-based gels. It is worth mentioning that fitting the experimental curve of pure PEO with eqs 2 and 3 is not possible. This indicates that the formed structures in pure PEO in the gel state are very different from those of PR$_7$. This confirms the primordial role of α-CD rodlike tubes on the self-organization of PR$_7$.

To get more insight into the kinetics, both parameters A (which reflects the weight of the Gaussian form factor) and B (which reflects the weight of the bundle form factor) are
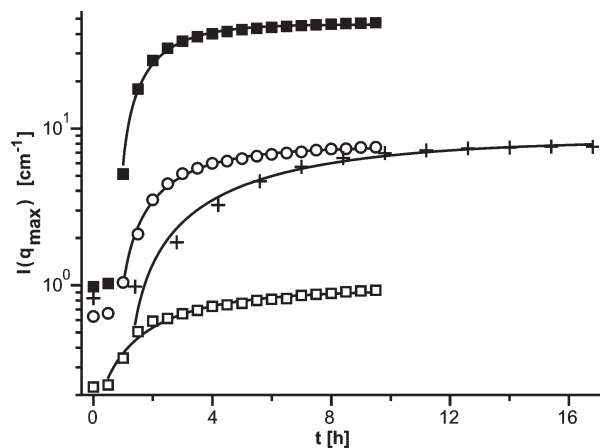
Figure 7. SANS: absolute scattering intensity I at $q_{max} = 3.63 \times 10^{-1}$ nm^{-1} versus time t at 21 °C and fitting curves obtained with eq 4 for PRs at 19.6% w/w in DMSO-d_6: (■) PR$_7$, (○) PR$_{37}$, (+) PR$_{85}$, and (□) PR$_{157}$.

studied. Figure 5b shows that A and B evolve according to the same temporal law:

$$y(t) = y_0 + y_\infty \left[1 - \exp\left(-\frac{t - \tau_0}{\tau_c} \right) \right] \qquad (4)$$

where y designates A or B, y_0 and y_∞ are values at short and long times, respectively, τ_0 is an induction time, and τ_c is a time characteristic of the evolution of the bundle number. The fitting values of τ_0 and τ_c are identical up to the temporal resolution of the acquisitions: $\tau_0 = 1.02$ h for A and 0.98 h for B, and $\tau_c = 1.52$ h for A and 1.33 h for B. This behavior suggests that the formation of aggregated α-CD rodlike tube domains is induced by the crystallization of naked PEO segments.

At Higher Complexation Degree N. At higher complexation degree, the physical gelation of PR solutions implies indubitably structures based on α-CD rodlike tubes and naked PEO segments as shown by differential scanning calorimetry (DSC), ^{1}H nuclear magnetic resonance (^{1}H NMR), and wide-angle X-ray scattering (WAXS).[21] Moreover, we demonstrated that the contribution of α-CD rodlike tubes to the association is more pronounced at higher N value.[21] However, as studied above, the contribution of α-CD rodlike tubes to the self-organization at the nanoscale exists for the lowest studied N value ($N = 7$).

The SANS profiles of PR$_{37}$, PR$_{85}$, and PR$_{157}$ are similar to the one obtained for PR$_7$ (Figure 7). Whatever the complexation degree N, eqs 2 and 3 well fit the experimental intensity profiles with the same bundle sizes ($L = 14$ nm and $R = 5.7$ nm) as the ones obtained for PR$_7$. For all studied PRs, the values of q_{max} and q'_{max} are constant. Moreover, whatever N, the most pronounced evolution with time of the Kratky plot consists in the growing of the peak at q_{max} as shown in Figure 5a. The profiles of the scattering intensity at $q_{max} = (3.63 \pm 0.3) \times 10^{-1}$ nm^{-1} versus time at 21 °C are of the same type for all studied PRs (Figure 7) and have the same shape as those shown in Figure 5b. The evolution of $I(q_{max})$ as a function of time is also well described by eq 4 (Figure 7). For all PR solutions, the times τ_0 and τ_c are in agreement with those obtained when fitting the time-dependent parameter B reflecting the weight of the bundle form factor of eq 2.

In the following, we consider the evolution of the characteristic time τ_c as a function of the complexation degree
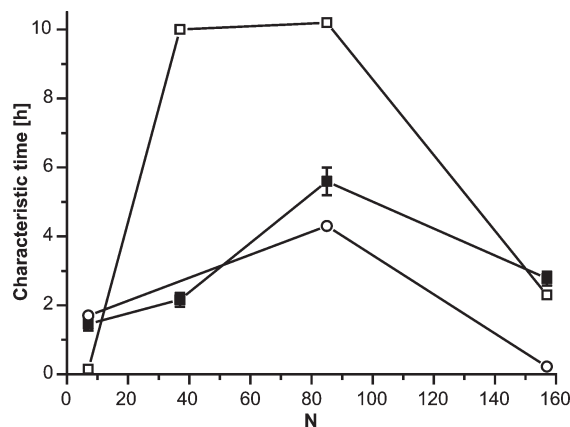

Figure 8. (■) Characteristic time τ_c determined through SANS measurements, (□) characteristic time τ_c determined through RDA measurements, and (○) characteristic time τ_c'' determined through DSC measurements versus complexation degree N for PRs at 19.6% w/w in DMSO-d_6 at 21 °C.

N (Figure 8). The time τ_c does not show a monotonous evolution with N. At low N values, the intrinsic flexibility of PRs is high due to long naked PEO segments, leading to a self-organization which is kinetically favored. Furthermore, at constant PR weight fraction, the number of PR molecules is the highest at the lowest N value (Table 1), increasing the bundle number. At high N values, PRs are more rigid, as observed for PR$_{157}$, leading to rapid prealignment of the PR molecules.

Characteristic times were also determined through RDA and DSC measurements.[21] The times determined through RDA are higher than those obtained by DSC and SANS (Figure 8). Indeed, RDA measurements probe the elasticity of the gel and thus are little sensitive to the first stages of the aggregation, before percolation is reached. On the opposite, DSC measurements are sensitive to all types of aggregation events, whatever their size or structure, and lead thus to the fastest kinetics. SANS measurements which highlight the formation of well-defined structures lead to intermediate characteristic times.

4. Conclusion

The structure of PRs based on α-CDs threaded onto 22 kg mol^{-1} PEO chains in concentrated solution ($\approx 20\%$ w/w) in DMSO was studied by SANS measurements as a function of the temperature and the complexation degree N which ranged from 7 up to 157. Furthermore, the behavior of a pure PEO solution in DMSO (at 5.9% w/w) was also compared with the one of PRs. At 43 °C, the PEO and all PR solutions stay liquid. Whereas SANS showed isolated flexible Gaussian chains in the pure PEO/DMSO mixture, a multiblock copolymers behavior was revealed for PRs in DMSO. This multiblock behavior of PRs at 43 °C is due to the presence of two kinds of blocks which alternate along the PR. One block type is rigid and corresponds to α-CD rodlike tubes with a length $L_{rod} \approx 7$ nm. The other block type corresponds to flexible naked PEO segments. For the highest N value (i.e., 157 corresponding to an α-CD overlap ratio $\approx 63\%$), the PR is much more rigid and showed rods longer than 45 nm, which is in the same order as the developed length of the 22 kg mol^{-1} PEO chain.

When the PEO or the PR mixtures are cooled down to 21 °C, they gelify slowly with time. Whereas the PEO/DMSO forms a macroscopic heterogeneous gel, the PR/DMSO physical gels are homogeneous and transparent to the eyes at room temperature. For the PEO/DMSO system, gelation is due to large aggregates constituted by the gathering of small nanoscale crystallites.

The gel structure is due to the multiblock copolymer behavior of PRs leading to the formation of regular bundles for which the characteristic sizes (L = 14 nm and R = 5.7 nm) are constant during the gelation process and are independent of N. These regular bundles contain naked PEO segment crystallites surrounded by α-CD rodlike tube aggregates at their extremities. Indeed, α-CD rodlike tubes, which are present in the initial state at 43 °C, act like a compatibilizer and thus lead to the nanoscale bundle sizes and, in contrast with the PEO/DMSO system, to the transparency of the physical PR-based gels. Furthermore, we showed that the kinetics of the bundle formation is N-dependent. Indeed, at constant PR weight fraction in DMSO, the N value is a crucial parameter controlling the intrinsic flexibility of PRs (flexibility favored at low N values) and their prealignment (prealignment favored at high N values) and thus controlling the self-organization.

Supporting Information Available: Sensitivity of SANS measurements in DMSO-d_6. This material is available free of charge via the Internet at http://pubs.acs.org.

References and Notes

(1) Harada, A.; Li, J.; Kamachi, M. *Nature* **1992**, *356*, 325–327.
(2) Wenz, G.; Keller, B. *Angew. Chem., Int. Ed. Engl.* **1992**, *31*, 197–199.
(3) Okumura, Y.; Ito, K. *Adv. Mater.* **2001**, *13*, 485–487.
(4) Fleury, G.; Schlatter, G.; Brochon, C.; Hadziioannou, G. *Polymer* **2005**, *46*, 8494–8501.
(5) Sakai, T.; Murayama, H.; Nagano, S.; Takeoka, Y.; Kidowaki, M.; Ito, K.; Seki, T. *Adv. Mater.* **2007**, *19*, 2023–2025.
(6) Fleury, G.; Schlatter, G.; Brochon, C.; Travelet, C.; Lapp, A.; Lindner, P.; Hadziioannou, G. *Macromolecules* **2007**, *40*, 535–543.
(7) Fleury, G.; Schlatter, G.; Brochon, C.; Hadziioannou, G. *Adv. Mater.* **2006**, *18*, 2847–2851.
(8) Karino, T.; Shibayama, M.; Ito, K. *Phys. B: Condens. Matter* **2006**, *385−386*, 692–696.
(9) Ito, K. *Polym. J.* **2007**, *39*, 489–499.
(10) Shimomura, T.; Akai, T.; Abe, T.; Ito, K. *J. Chem. Phys.* **2002**, *116*, 1753–1756.
(11) van den Boogaard, M.; Bonnet, G.; van't Hof, P.; Wang, Y.; Brochon, C.; van Hutten, P.; Lapp, A.; Hadziioannou, G. *Chem. Mater.* **2004**, *16*, 4383–4385.
(12) Ooya, T.; Yui, N. *J. Controlled Release* **2002**, *80*, 219–228.
(13) Wenz, G.; Han, B.-H.; Müller, A. *Chem. Rev.* **2006**, *106*, 782–817.
(14) Ceccato, M.; Lo Nostro, P.; Baglioni, P. *Langmuir* **1997**, *13*, 2436–2439.
(15) Mayer, B.; Klein, C.; Topchieva, I.; Köhler, G. *J. Comput.-Aided Mol. Des.* **1999**, *13*, 373–383.
(16) Harada, A.; Li, J.; Nakamitsu, T.; Kamachi, M. *J. Org. Chem.* **1993**, *58*, 7524–7528.
(17) Harada, A.; Li, J.; Kamachi, M. *J. Am. Chem. Soc.* **1994**, *116*, 3192–3196.
(18) Samitsu, S.; Araki, J.; Kataoka, T.; Ito, K. *J. Polym. Sci., Part B: Polym. Phys.* **2006**, *44*, 1985–1994.
(19) Araki, J.; Kataoka, T.; Ito, K. *J. Appl. Polym. Sci.* **2007**, *105*, 2265–2270.
(20) Araki, J.; Ito, K. *J. Polym. Sci., Part A: Polym. Chem.* **2006**, *44*, 532–538.
(21) Travelet, C.; Schlatter, G.; Hébraud, P.; Brochon, C.; Lapp, A.; Anokin, D.; Ivanov, D.; Gaillard, C.; Hadziioannou, G. *Soft Matter* **2008**, *4*, 1855–1860.
(22) Travelet, C.; Schlatter, G.; Brochon, C.; Hébraud, P.; Ivanov, D.; Hadziioannou, G. CD-ROM Congress Proceedings of the EPF 2007, European Polymer Congress, Portorož (Slovenia), 2−6 July **2007**.
(23) Araki, J.; Ito, K. *Polymer* **2007**, *48*, 7139–7144.
(24) Fleury, G.; Brochon, C.; Schlatter, G.; Bonnet, G.; Lapp, A.; Hadziioannou, G. *Soft Matter* **2005**, *1*, 378–385.
(25) Mutter, M. *Tetrahedron Lett.* **1978**, *19*, 2839–2842.
(26) Brûlet, A.; Lairez, D.; Lapp, A.; Cotton, J.-P. *J. Appl. Crystallogr.* **2007**, *40*, 165–177.
(27) Harada, A. *Coord. Chem. Rev.* **1996**, *148*, 115–133.
(28) Harada, A. *Carbohydr. Polym.* **1997**, *34*, 183–188.
(29) Horský, J.; Porsch, B. *J. Inclusion Phenom. Macrocyclic Chem.* **2005**, *53*, 97–102.
(30) Fournet, G. *Bull. Soc. Fr. Mineral. Cristallogr.* **1951**, *74*, 37−167 (in French).
(31) Lindner, P.; Zemb, T. *Neutron, X-rays and Light: Scattering Methods Applied to Soft Condensed Matter*; Elsevier: Amsterdam, Netherlands, 2002.
(32) Debye, P. *J. Phys. Colloid Chem.* **1947**, *51*, 18–32.
(33) Szejtli, J. *Chem. Rev.* **1998**, *98*, 1743–1753.
(34) van den Boogaard, M. Cyclodextrin-containing Supramolecular Structures: from Pseudo-polyrotaxanes Towards Molecular Tubes, Insulated Molecular Wires and Topological Networks. Ph.D. Thesis, University of Groningen, Netherlands, **2003** (available via the Internet at http://irs.ub.rug.nl/ppn/24276326X or http://dissertations.ub.rug.nl/search.php).
(35) Girardeau, T.; Zhao, T.; Leisen, J.; Beckham, H.; Bucknall, D. *Macromolecules* **2005**, *38*, 2261–2270.
(36) Tonelli, A. *Macromolecules* **2008**, *41*, 4058–4060.
(37) Zhao, C.; Domon, Y.; Okumura, Y.; Okabe, S.; Shibayama, M.; Ito, K. *J. Phys.: Condens. Matter* **2005**, *17*, S2841–S2846.
(38) Mayumi, K.; Osaka, N.; Endo, H.; Yokoyama, H.; Sakai, Y.; Shibayama, M.; Ito, K. *Macromolecules* **2008**, *41*, 6480–6485.
(39) Auvray, L. *C. R. Acad. Sci.* **1986**, *302*, 859–862.
(40) Teixeira, J. *J. Appl. Crystallogr.* **1988**, *21*, 781–785.
(41) Williamson, D.; Marr, D.; Yang, J.; Yan, B.; Guha, S. *Phys. Rev. B: Condens. Matter Mater. Phys.* **2003**, *67*, 075314–1−075314−13.
(42) Bale, H.; Schmidt, P. *Phys. Rev. Lett.* **1984**, *53*, 596–599.